

A Generic Point Error Model for TLS Derived Point Clouds

Mustafa Ozendi^{1a}, Devrim Akca^b, Hüseyin Topan^a

^aBEU, Department of Geomatics Engineering, 67100 Zonguldak, Turkey;

^bIsik University, Department of Civil Engineering, 34980 Sile, Istanbul, Turkey

ABSTRACT

This work aims at developing a generic and anisotropic point error model, which is capable of computing magnitude and direction of a priori random errors, described in the form of error ellipsoids for each individual point of the cloud. The direct TLS observations are the range (ρ), vertical (α) and horizontal (θ) angles, each of which is in fact associated with a priori precision value. A practical methodology was designed and performed in real-world test environments to determine these precision values. The methodology has two experimental parts. The first part is a static and repetitive measurement configuration for the determination of a priori precisions of the vertical (σ_α) and horizontal (σ_θ) angles. The second part is the measurement of a test stand which contains four plates in white, light grey, dark grey and black colors, for the determination of a priori precisions of the range observations (σ_ρ). The test stand measurement is performed in a recursive manner so that sensor-to-object distance, incidence angle and surface reflectivity are parameterized. The experiment was conducted with three TLSs, namely Faro Focus 3D X330, Riegl VZ400 and Z+F 5010x in the same location and atmospheric conditions. This procedure was followed by the computation of error ellipsoids of each point using the law of variance-covariance propagation. The direction and size of the error ellipsoids were computed by the principal components transformation. Validation of the proposed error model was performed in real world scenarios, which revealed feasibility of the model.

Keywords: TLS (terrestrial laser scanner), range, incidence angle, reflectance, error ellipsoid, anisotropic, error model, variance-covariance propagation

1. INTRODUCTION

Terrestrial laser scanners (TLSs) capture the geometry of target object or scene accurately in the form of dense point clouds. Any point in the scan data is contaminated by the random errors. These errors propagate through the steps of data processing, namely pre-processing, co-registration, mesh integration and 3D model reconstruction. Therefore, estimating the random error pattern of every individual point is essentially important for validating TLS derived 3D models. The range of applications are various such as surface matching [1, 2], 3D object modeling and surface mesh generation [3-5], and surface comparison [6, 7].

The random error pattern can be investigated by means of positional uncertainty which is influenced by multiple parameters. Angular (mechanical) stability, sensor-to object distance, incidence angle of the incoming laser beam, and surface reflectivity are the most significant ones. This fact results in a heteroscedastic (point dependent), anisotropic and inhomogeneous point error distribution [8-10], which states that the positional uncertainty of each point is different.

The basic TLS observations are the range (i.e. sensor-to-object distance), horizontal and vertical angles. In addition TLSs can measure the amplitude of the reflected laser beam or so called intensity which is a quantity of the reflectivity of the object surface. The precision of the range measurement was theoretically approximated by Hebert and Krotkov [11] considering physical, optical and electronic characteristics of the sensor and reflectivity of the observed scene. It was shown that this model is not sufficient in practice [12]. An additive error model was presented in Williams et al. [10] to improve the co-registration quality by means of the covariance matrix of points. Another covariance matrix based anisotropic error model was developed for a commercial structured light system which uses the photogrammetric collinearity equations in point positioning [13]. While the error model proposed by Okatani and Deguchi [14] fundamentally considers the range measurement error, it omits the angular measurement errors. The scan data was smoothed depending on the variance of each point. A similar approach was used in Sagawa et al. [15] to refine data

¹ mustafa.ozendi@beun.edu.tr

iteratively, similar to the ICP algorithm. This approach was further improved in estimating the uncertainty by relating the ranging precision and the amplitude of the reflected light [16, 17]. For stochastic modelling, precision values provided by the manufacturer can be used to compute covariance matrix of each point [18]. However, such an approach will not yield a point dependent error model because each point will have the same value. Moreover, incidence angle and surface reflectivity parameters are not considered in this method. In Bae et al. [19] the effect of the incidence angle on the ranging precision was reported. This approach can hardly be implemented in practice.

The incidence angle of the incoming laser beam has a significant effect on the range precision. This effect can be quantified as the cosine of the incidence angle as reported by Soudarissanane et al. [20]. This formulation was advanced in order to compute point-wise covariance matrices provided that the manufacturer precision values are available [21]. Moreover, the same formulation can be used in the surface reconstruction related studies [22]. The point cloud precision was alternatively evaluated by means of the error ellipsoids [23, 24]. Schaer et al. [25] extended the state-of-the-art computations so that the effect of laser spot (foot print) was also considered in addition to vendor provided precision numbers and incident angle. However, reflectivity of object surface and the linearity error of range were not included in the computations. Mezian et al. [26] developed a positional uncertainty model specifically for the mobile terrestrial LiDAR sensors. Their model estimates the error ellipsoids of each point using the vendor provided precision numbers, meanwhile neglecting the effects of incidence angle and surface reflectivity. In a recent study, precision of distance measurement of a Z+F Imager 5006 TLS was stochastically modelled using raw intensity values [27]. However, this model cannot be used for the TLSs which do not provide the raw intensity values, publicly.

Such a large number of studies show the relevance of the problem. A fully satisfying solution, which mathematically formulates the physical nature of the instrumental and environmental errors, has to be still designed, realized and justified. This paper presents a generic and anisotropic point error model, which is capable of computing magnitude and direction of a priori random errors, described in the form of error ellipsoids which are associated with every individual point of the cloud. Unlike the referenced studies, the proposed point error model includes a priori precision values of range and angular (horizontal and vertical) observations. In addition, a mathematical model was developed for the range precision considering the most falsifying parameters, namely the distance between TLS and target object, incidence angle of the incoming laser beam and surface reflectivity. The following section summarizes the theoretical background of the generic point error model. Section 3 describes the determination of a priori angular and range precision. Section 4 presents the usability and feasibility of the proposed error model and finally, in Section 5, conclusions are reported.

2. THEORETICAL BACKGROUND OF THE ANISOTROPIC POINT ERROR MODEL

The TLS systems operate in a spherical coordinate system measuring the range (ρ), vertical (α) and horizontal (θ) angles as the direct observations (Figure 1).

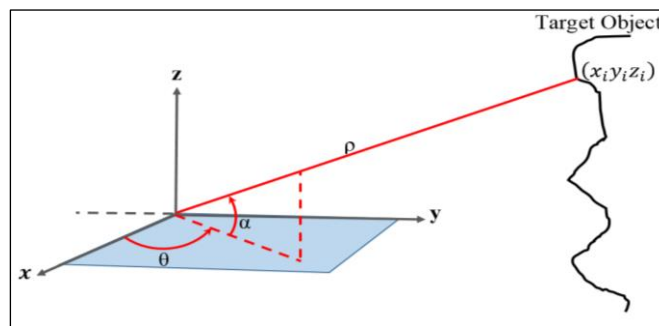


Figure 1. The direct observations of a TLS system.

Any point is defined as $r_i = [\rho_i \alpha_i \theta_i]^T$ where $i = 1, 2, \dots, n$ is the number of points in the data set. The Cartesian coordinates $[x_i \ y_i \ z_i]^T$ of any i -th point can be computed from the spherical observations $r_i = [\rho_i \alpha_i \theta_i]^T$ as:

$$\begin{bmatrix} x_i \\ y_i \\ z_i \end{bmatrix} = \begin{bmatrix} \rho_i \cos(\alpha_i) \cos(\theta_i) \\ \rho_i \cos(\alpha_i) \sin(\theta_i) \\ \rho_i \sin(\alpha_i) \end{bmatrix} \quad (1)$$

Transformation from the Cartesian coordinates $[x_i \ y_i \ z_i]^T$ to the spherical coordinates $[\rho_i \ \alpha_i \ \theta_i]^T$ can be performed using the following equations:

$$\rho = \sqrt{x^2 + y^2 + z^2} \quad (2)$$

$$\alpha = \tan^{-1} \left(\frac{z}{\sqrt{x^2 + y^2}} \right) \quad (3)$$

$$\theta = \tan^{-1} \left(\frac{y}{x} \right) \quad (4)$$

The covariance matrix of any point r_i can be established using the a priori precision values as follow:

$$\Sigma_{rr} = \begin{bmatrix} \sigma_\rho^2 & 0 & 0 \\ 0 & \sigma_\alpha^2 & 0 \\ 0 & 0 & \sigma_\theta^2 \end{bmatrix} \quad (5)$$

where, σ_ρ^2 , σ_α^2 and σ_θ^2 represent a priori variances of the range (ρ), vertical (α) and horizontal (θ) angles, respectively. Non-diagonal elements of this matrix are zero under the assumptions;

- The TLS is well-calibrated, thus the range and angular measurements are free of systematic errors,
- There is no physical correlation between the direct observations.

The second assumption is valid since the range and angle measurement units are independent from the each other. The range measurement is performed with using either time of flight or phase measurement technique through the optical telescope system. The angle measurements are performed electro optically by high resolution vertical and horizontal angular encoders which are physically separated from the each other [28, 29].

Using the law of error propagation, the covariance matrix Σ_{xx} of a point in the Cartesian coordinate system is:

$$\Sigma_{xx} = J_{xr} \Sigma_{rr} J_{xr}^T \quad (6)$$

where J_{xr} is the Jacobian matrix of the partial derivatives of the Cartesian coordinates with respect to the range (ρ), vertical (α) and horizontal (θ) angle observations as shown in Equation (7).

$$J_{xr} = \begin{bmatrix} \frac{\partial x}{\partial \rho} & \frac{\partial x}{\partial \alpha} & \frac{\partial x}{\partial \theta} \\ \frac{\partial y}{\partial \rho} & \frac{\partial y}{\partial \alpha} & \frac{\partial y}{\partial \theta} \\ \frac{\partial z}{\partial \rho} & \frac{\partial z}{\partial \alpha} & \frac{\partial z}{\partial \theta} \end{bmatrix} \quad (7)$$

The parameters of the error ellipsoid can be calculated from the principal components of the variance-covariance matrix Σ_{xx} as shown in Equation (8).

$$(\Sigma_{xx} - \lambda I)z = 0 \quad (8)$$

Here, I is the unit matrix, $\lambda = [\lambda_1, \lambda_2, \lambda_3]$ are the eigenvalues and $z = [z_1 \ z_2 \ z_3]$ is the eigenvector of the covariance matrix Σ_{xx} .

The dimensions of the semi- axes of the error ellipsoid are the square root of the eigenvalues ($\sqrt{\lambda_1}, \sqrt{\lambda_2}, \sqrt{\lambda_3}$). The axes orientations of the ellipsoids are given by the eigenvectors $z = [z_1 \ z_2 \ z_3]$. Vertical and horizontal directions can be computed as shown in Equation (9).

$$\begin{aligned} \text{Vertical Direction} &= \tan^{-1} \left(\frac{z_3}{\sqrt{z_1^2 + z_2^2}} \right) \\ \text{Horizontal Direction} &= \tan^{-1} \left(\frac{z_1}{z_2} \right) \end{aligned} \quad (9)$$

The error ellipsoids fictitiously represent the magnitude and direction of the random error of the associated point. At this step, the error ellipsoid of every individual point can be computed provided that a priori precision values of the direct measurements ($\sigma_\rho, \sigma_\alpha, \sigma_\theta$) in Equation (5) are given. We developed a practical methodology for the determination of such a priori precision values, which is explained in the following section.

3. DETERMINATION OF A PRIORI PRECISION VALUES: A PRACTICAL METHODOLOGY

The range, vertical angle and horizontal angle are the direct observations of a TLS, which obviously have their own a priori precision values. Since the TLS manufacturers do not publicly or standardly share these values, we designed and realized a practical methodology in order to determine them. The methodology does not require specific laboratory conditions and equipment; rather it is practical so that it can be conducted at real world environments. As the range measurement varies in a certain sight-of-line direction, the vertical and horizontal angle measurements remain the same. Thus, the ranging mechanism of the TLS does not have any effect on the angular precision [29]. Therefore, we factorize determination of the angular precision and the range precision tasks into two separate experimental parts.

The first part is a static and repetitive measurement configuration for the determination of a priori precision values of the vertical (σ_α) and horizontal (σ_θ) angles.

Consequently, the second part is the measurement of a test stand which contains four plates in white, light gray, dark gray and black colors for the determination of a priori precisions of the range observations (σ_ρ). The test stand measurements were performed in a recursive manner so that sensor-to-object distance, incidence angle and surface reflectivity are parameterized.

All experiments were conducted almost in the same atmospheric conditions for three different TLSs, namely Faro Focus 3D X330, Riegl VZ400 and Z+F 5010x. All the scanners were set to a moderate resolution and quality level. The technical specifications are summarized in Table 1.

Table 1. Technical specifications of the tested TLS systems.

			
	Faro Focus 3D X330	Riegl VZ400	Z+F 5010x
Laser Class	Laser Class 1	Laser Class 1	Laser Class 1
Range Measurement Error	±2mm @ 25-50m	±3mm @ 100m	Linearity Error ≤ 1mm
Ranging Method	Phase Measurement	Time of flight	Phase Measurement
Beam Divergence	121.0 ^{cc} (0.19 mrad)	222.8 ^{cc} (0.35 mrad)	<191.0 ^{cc} (0.30 mrad)
Wavelength	1550nm	Near Infrared	1500nm
Angular Step Width (Hor.)	100 ^{cc}	26.7 ^{cc}	2.2 ^{cc}
Angular Step Width (Ver.)	100 ^{cc}	26.7 ^{cc}	4.4 ^{cc}
Field of View (Ver./Hor.)	333.3 ^g / 400 ^g	111.1 ^g / 400 ^g	355.6 ^g / 400 ^g

3.1 Angular precisions (σ_α and σ_θ) determination

The angular precisions of a TLS can be defined as the repeatability of the angle observations. The vertical and horizontal angle measurements are independent from the object space conditions, such as temperature, surface reflectivity, distance, etc. Rather, they are the result of mechanical movements of the laser beamer along the vertical and horizontal directions, respectively. It is a mechanical stability problem. The higher the precision, the lesser the scatter of the vertical and horizontal angle values coming from the repetitive scans.

The vertical and horizontal angle precisions are assessed by the repeated scans of the same environment when the TLS is set up firmly static. In our case, the same environment was scanned five times from the same station. The repetitive scans were performed with four-to-six minute time intervals to verify that the TLS is exactly stable, and heating and cooling of the device is at moderate level. It is expected that each point should coincide with its conjugates in the other scans. The five conjugate points of the same laser ray are shown in Figure 2a, 2b and 2c for the Faro, Riegl and Z+F scanners, respectively.

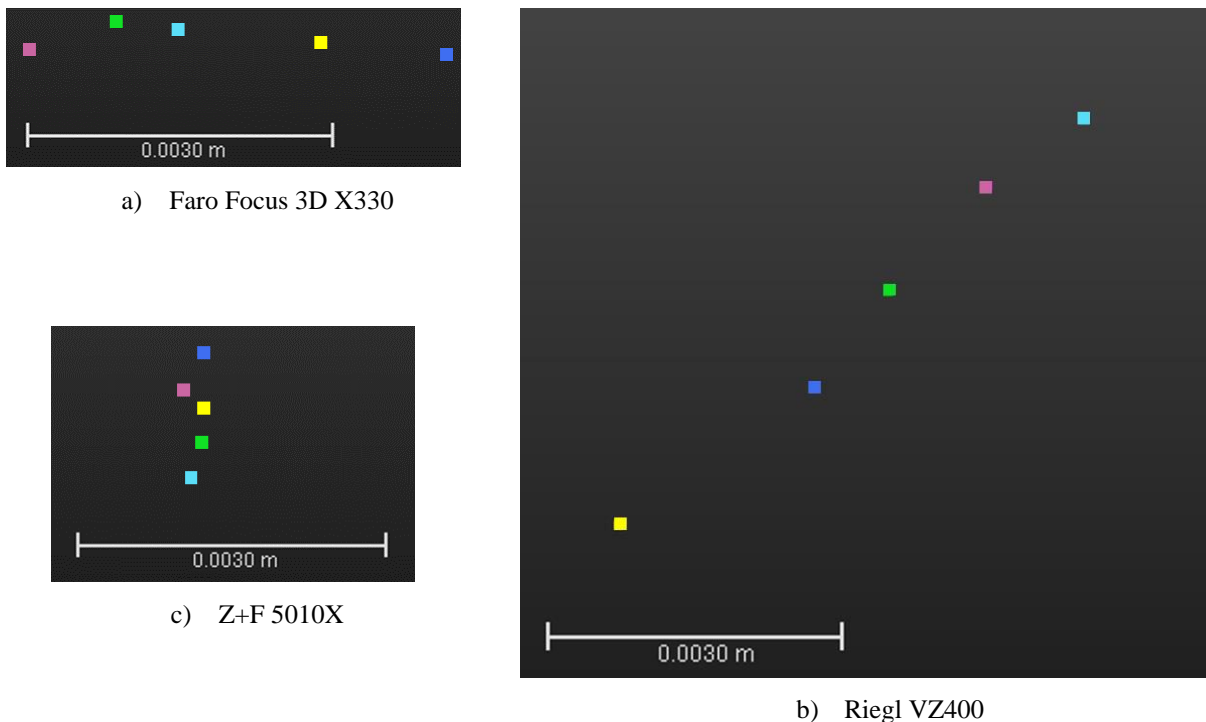


Figure 2. Distribution of the conjugate points of a laser ray as a result of five repeated scans. The views are rendered along the lateral direction. The ordinate is the vertical angle direction and the abscissa is the horizontal angle direction.

The 1st, 2nd, 3rd, 4th and 5th scan points are depicted in yellow, green, cyan, blue and purple colors, respectively. It is clear that angular precisions of the three scanners are not equivalent along the vertical and horizontal directions both in terms of magnitude and direction. The Faro scanner exhibits a better vertical angle precision than the horizontal angle. The situation at Z+F scanner is completely vice-versa. The Riegl scanner shows similar precisions both for the horizontal and vertical angles, although with larger magnitudes than the Faro and Z+F (Figure 2). The same patterns for the same scanners were observed in other conjugate points at different directions. Therefore, a priori precisions of the vertical (σ_α) and horizontal (σ_θ) angles are the scanner variant numbers, and not the point variant.

The deviations of the conjugate points are relevant to the angular repeatability of the scanner system. The five conjugate points of the same laser ray were selected and corresponding vertical (α) and horizontal (θ) angles were computed using Equations (3) and (4). The root mean square error (RMSE) values of these angular discrepancies were computed. This RMSE computation was repeated at least four laser rays which towards the four main directions. The mathematical mean of these four RMSE values yields the a priori angular precisions. This procedure was carried out for all the three scanners. As a result, the final precision values of the vertical and horizontal angles (σ_α and σ_θ) are tabulated in Table 2.

The Z+F scanner has the least vertical and horizontal step widths (Table 1), and accordingly the least vertical and horizontal angle precision numbers (Table 2). The same relation does not exist between the Faro and Riegl scanners. Although the Riegl scanner has five times less step width values than the Faro scanner, the Faro scanner has considerably better precision values. This is due to the better internal stability of the Faro scanner.

Table 2. Angular Precision Values.

Faro Focus 3D x 330		Riegl VZ 400		Z+F 5010x	
σ_α	σ_θ	σ_α	σ_θ	σ_α	σ_θ
18.8 ^{cc}	76.2 ^{cc}	94.5 ^{cc}	107.2 ^{cc}	26.7 ^{cc}	3.8 ^{cc}

The angular precisions of the TLSs have been already investigated in the previous studies [29-31]. The repeated measurements method is the mostly used one. The results of our study are consistent with the previous studies.

3.2 Range precision (σ_ρ) determination

The range precision (σ_ρ) depends not only the sensor space (instrumental) parameters but also many object space (environmental) parameters. Among them, the most effective ones are the distance from TLS to object, incidence angle of the incoming laser beam, and reflectivity of object surface. Thus, the range precision is point variant, and should be determined for each point individually. In order to determine a priori range precision (σ_ρ) of the points, a test stand, which is compliant with both indoor and outdoor usage, was constructed (Figure 3a).

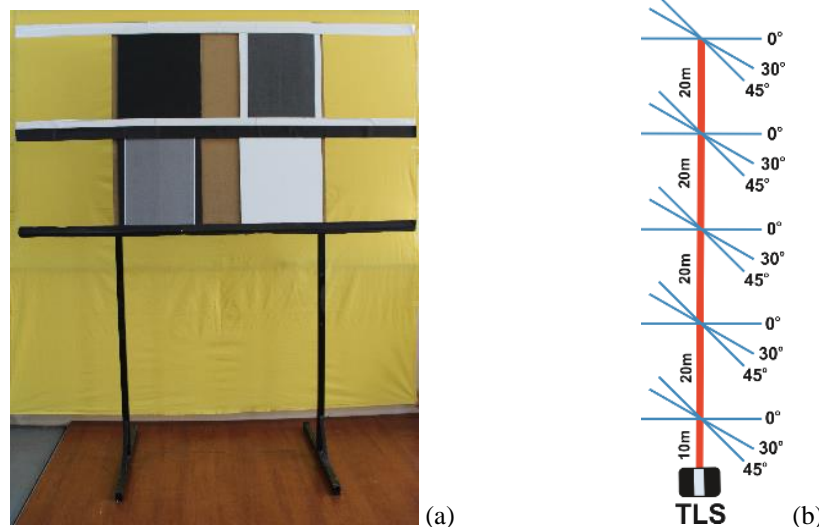


Figure 3. (a) The test stand containing the plates in white, light gray, dark gray and black colors. (b) The scan plan showing the top view of the experiment configuration. The locations and orientations of the test stand are represented with the blue lines.

The test stand consists of four glass plates on which A3 sized papers are glued with different reflectance properties, for which covering a wide spectrum of the intensity values. The white one is an ordinary unprinted paper. The light and dark gray papers were printed by a laser printer. The black one is sprayed with a fully black (matte) spray in order to absorb the large extend of the incoming beam. The test stand was placed at distances from the scanner ranging from 10m to 90m in steps of 20m (Figure 3b). At each step, the test stand was positioned with 0°, 30° and 45° orientation angles with respect to the TLS so that it enables investigation of the effects of the distance, incidence angle and reflectivity.

Four-to-six minutes time delays were given in between the consecutive scans to make sure that the scanner cooled the temperature down. A total of 15 scans of the test stand were acquired for each of the three scanners. Such an experiment

configuration allows for parameterization of the sensor-to-object distance, incidence angle and surface reflectivity, simultaneously.

Once the measurements were completed, data points on the plates were cropped and saved in separate files. Assuming that the plates are exactly planar, the least squares plane fitting was computed for each plate using the conventional least squares parameter estimation method. The following plane equation was employed

$$Ax_i + By_i + Cz_i + D = 0 \tag{10}$$

where A, B, C and D are the coefficients of the respective plane and (x_i, y_i, z_i) represent the coordinates of the points which lies in the plane. After the four plane coefficients were computed using the redundant point observations, off-plane distance (d_i) of every i -th scan point was computed using Equation (11).

$$d_i = \frac{Ax_i + By_i + Cz_i + D}{\sqrt{A^2 + B^2 + C^2}} \tag{11}$$

The RMSE of the off-plane distances d_i was computed, represented with the symbol (m), and considered as the empirical (data driven) a priori precision (σ_ρ) of the range measurements.

$$m = \pm \sqrt{\frac{\sum d_i d_i}{n-1}} \tag{12}$$

The (m) values of each plate at varying distances (10, 30, 50, 70 and 90 meters), orientation angles (0, 30 and 45 degrees) and reflectivity (black, dark gray, light gray and white papers) were computed. This procedure was repeated for each of those three scanners Faro, Riegl and Z+F and graphically depicted in Figures 4, 5 and 6, respectively.

Figures 4, 5 and 6 clearly demonstrate how the range precision σ_ρ changes when the distance, laser incidence angle and surface reflectivity change. Moreover, σ_ρ of the black objects get worse when compared to objects with gray and white colors. The incidence angle of the laser ray is another dominating factor deteriorating the point-positioning quality, especially for the black objects. On the other hand, perturbation of σ_ρ for dark gray, light gray and white objects are small. The point quality and quantity was so bad for the black plates of Z+F 5010X scanner at 90m 30°, 90m 45° and 70m 45° distances and orientation angles, respectively, the m values were not able to be calculated (Figure 6).

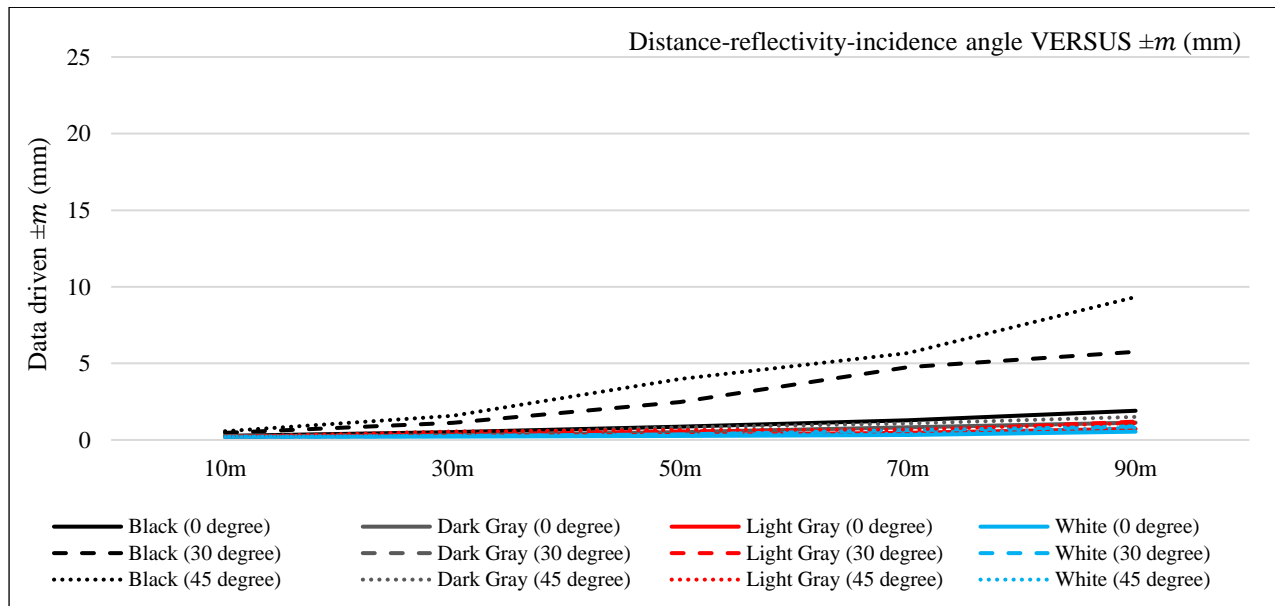


Figure 4. Data driven empirical σ_ρ values for the Faro Focus 3D X330 scanner.

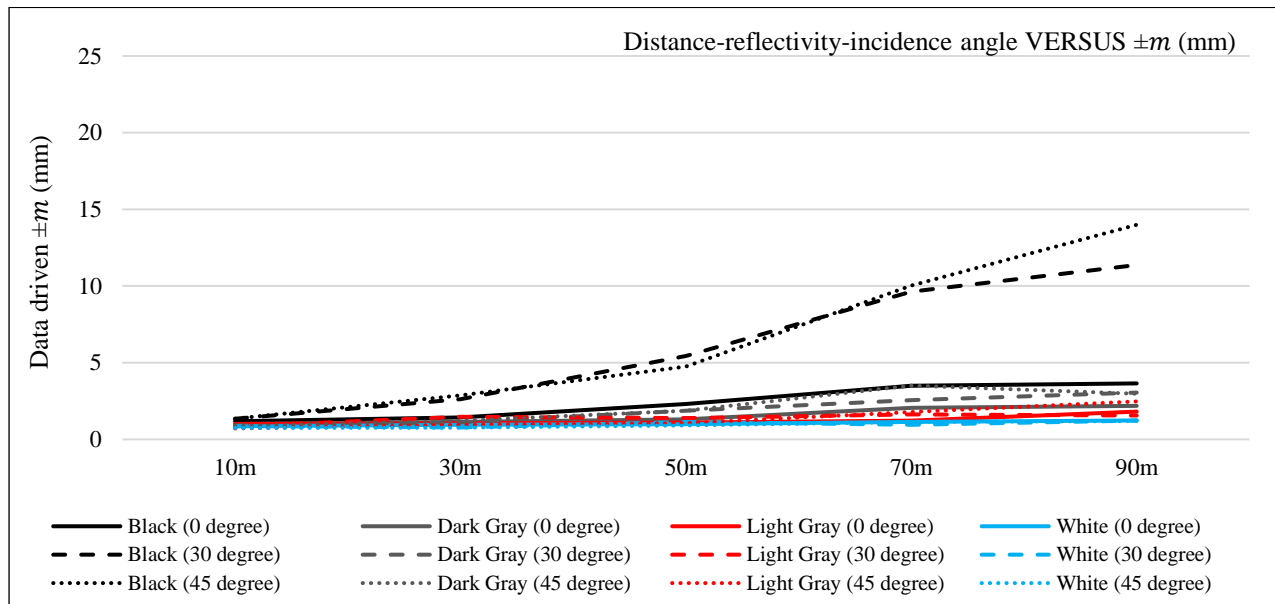


Figure 5. Data driven empirical σ_p values for the Riegl VZ400 scanner.

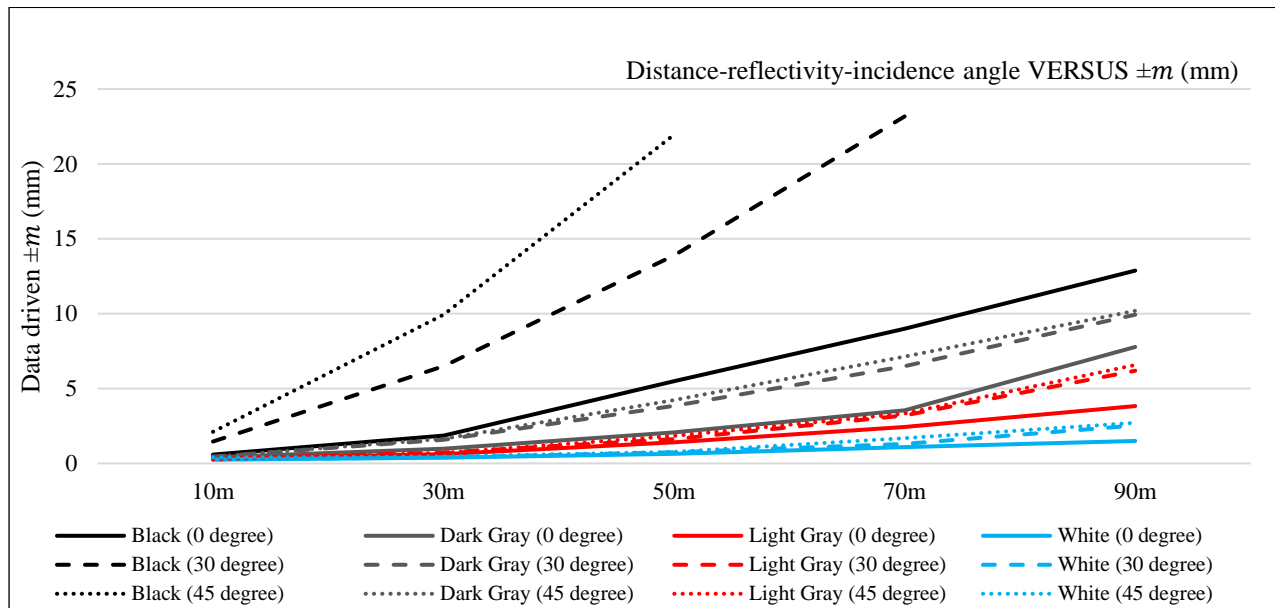


Figure 6. Data driven empirical σ_p values for the Z+F 5010X scanner.

Figures 4, 5 and 6 are rendered using the data driven method. Each figure requires 15 scan data of the pre-fabricated test stand. This empirical workload is heavy and not practical for ordinary scanning projects. We need a model driven method in order to determine the range precision σ_p with an appropriate mathematical model and less fieldwork. The following subsection explains such a method.

3.2.1 Model driven range precision (σ_ρ) determination

In the previous section, it has been demonstrated that there is a strong relation between the range precision (σ_ρ) and the object-space parameters which are the scanner-to-target distance (ρ), incidence angle (γ) and target reflectivity (I). The distance (ρ) and the incidence angle (γ) are computed through the Cartesian coordinates. The target reflectivity (I) is a measure of the intensity value of the returning signal. The range precision σ_ρ is unique for each point and can be formulated as a function of (ρ, γ, I). This model driven formula has to fulfil the following conditions:

- As the distance increases, σ_ρ increases linearly.
- As the incidence angle increases, the returned signal weakens which results in deterioration of σ_ρ . The degree of the deterioration is a factor of $\frac{1}{\cos(\gamma)}$ function [20-22].
- As the surface reflectivity is low, so as the target surface absorbs much of the incoming laser light, σ_ρ increases non-linearly as a quadratic function of the distance.

These conditions are the results of the analysis of the trend patterns of m values given in data driven graphics in Figures 4, 5 and 6.

Based on these conclusions, we developed the following formula for the model driven range precision (σ_ρ):

$$\sigma_\rho = \frac{c + (d * \rho) + f(I)}{\cos(\gamma)} \quad (13)$$

and

$$f(I) = \begin{cases} a + b * \rho^2 & , \text{ for } I < I_T^b \\ 0 & , \text{ elsewhere} \end{cases} \quad (14)$$

where a, b, c and d are the coefficients, ρ is the scanner-to-point distance, γ is the incidence angle and I is the intensity value. If provided by the associated software of the scanner, we prefer to use the reflectance value, which is the normalized and distance effect eliminated version of the intensity value. The coefficients a, b, c and d are constant for each scanner and the direct observations (ρ, γ, I) are variable for each point.

The equation part $c + (d * \rho)$ is the linear distance error where c is the constant error and d is the slope of the regression line. The function $f(I)$ is the error contribution of the target reflectivity. It is a quadratic function of the distance. The cubic or linear functions can also be considered. The linear distance error and the target reflectivity error are the additive terms. The denominator term $\cos(\gamma)$ is the error due to the incidence angle, which intensify or attenuate the additive error terms.

The coefficients a, b, c and d are the scanner (sensor space) parameters which can be derived by means of a simplified experimental set up, instead of conducting the full extent of the fieldwork experiment (Figure 3a and 3b). This simplified experimental set up requires two highly absorbent planar objects (black plates) and two highly reflective planar objects (white plates). The black and white plates can be scanned at close and far distances such as at 10 and 90 meters, respectively. Their orientations are kept perpendicular to the TLS so that the incidence angles become zero degrees. This simplified experiment configuration is sufficiently enough to recover the scanner variant a, b, c and d parameters. The four m values (RMS error of the off-plane distances) are calculated using Equation (12) for the first set of black-and-white-plates located at 10 meter and the second set located at 90 meter. A hypothetical graph is plotted in Figure 7.

In Figure 7, ordinate values m stand for RMSE of the off-plane distances, where the subscript means the distance between TLS to plate (10 or 90) and the superscript means color of the plate (b (black) or w (white)). The scanner variant parameters a, b, c and d of Equations (13) and (14) are computed by the following steps:

- The parameter c is the constant error of the TLS, which is amount of the shift of the line of the white plates (red line in Figure 7) from the range axis (abscissa). Parameter c is the summation of the constant distance accuracy (e) provided by the manufacturer and m_{10}^w which is the intercept of the red line.

$$c = e + m_{10}^w \quad (15)$$

- The parameter d is the slope of the red line (Figure 7) and can be computed as in Equation 16, which is a kind of linear interpolation. Although the formula is defined to start from the close distance 10 meter, it is straightforwardly applied for the points whose distances are $\rho < 10$ meter. The discrepancies are minor, and do not change the results significantly.

$$d = \frac{m_{90}^w - m_{10}^w}{90 - 10} = \tan(\beta) \quad (16)$$

- The parameters a and b can be calculated by solving the following equation system:

$$\begin{aligned} a + b * 10^2 &= m_{10}^b - m_{10}^w \\ a + b * 90^2 &= m_{90}^b - m_{90}^w \end{aligned} \quad (17)$$

- I_T^b is the threshold for the black reflectance values. If the reflectance value (I) of any point is smaller than the threshold I_T^b , the a priori precision value is attenuated as much as the function $f(I)$ as shown in Equation 13. The threshold I_T^b is defined as the maximum of the average reflectance values belonging to the black plates positioned at 90m and 10m away from the TLS.

$$I_T^b = \max\{I_{90m}^b, I_{10m}^b\} \quad (18)$$

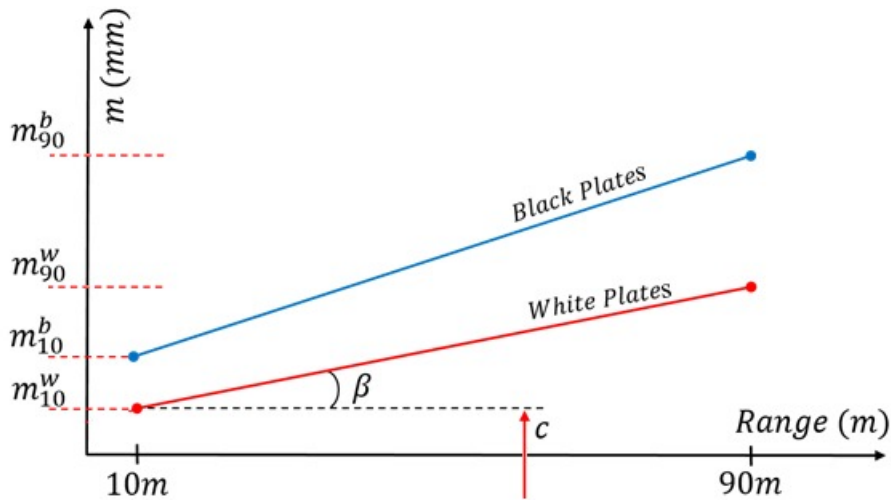


Figure 7. Two sets of the black-and-white-plates are located at 10 and 90 meters distances, respectively. All of the four plates are at the rotation of 0 degrees of incidence angles.

The experiment and associated computations (Equations 13-18) have been conducted for all of the three scanners. Our computed parameters are given in Table 3. The threshold I_T^b values are the large numbers for the Faro and Riegl scanners, as their reflectance numbers are over exposed and their histograms are non-symmetric.

Table 3. Parameters of the model driven a priori range precision formula for the three scanners.

TLS brand	a	b	d	e (mm)	m_{10}^w (mm)	I_T^b [0-255] gray level
Faro Focus 3D X330	0.042	0.000163	0.0042	2	0.21	191
Riegl VZ400	0.297	0.000262	0.0047	3	0.86	133
Z+F 5010X	0.203	0.001380	0.0157	1	0.25	23

Once the coefficients a, b, c and d are computed, the model-driven range precision σ_p is calculated with the formula given in Equations (13) and (14) using the functions of (ρ, γ, I) variables. These model driven σ_p values are plotted in Figures 8, 9 and 10 for comparison with the data driven σ_p values given in Figures 4, 5 and 6.

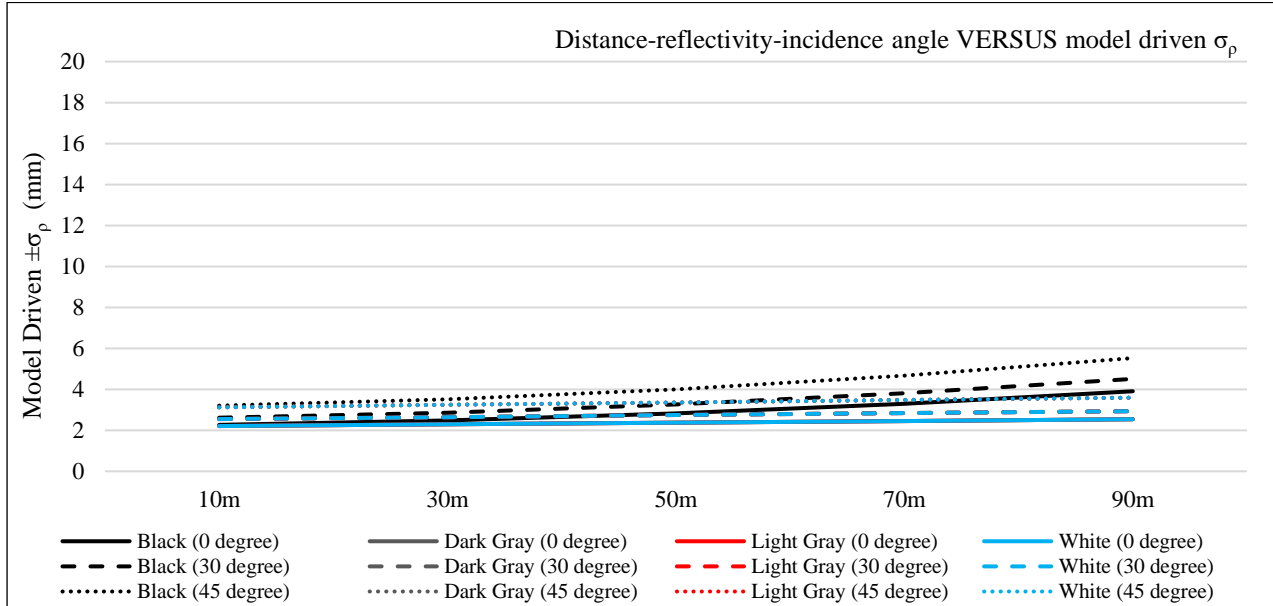


Figure 8. Model driven σ_p values for the Faro Focus 3D X330 scanner.

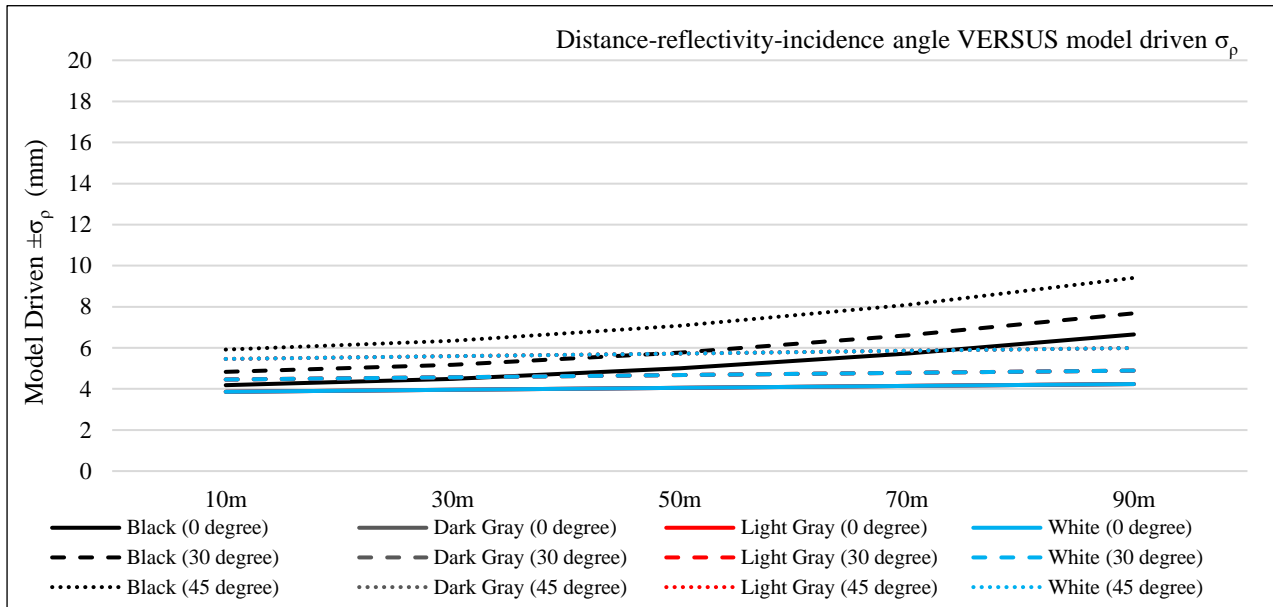


Figure 9. Model driven σ_p values for the Riegl VZ400 scanner.

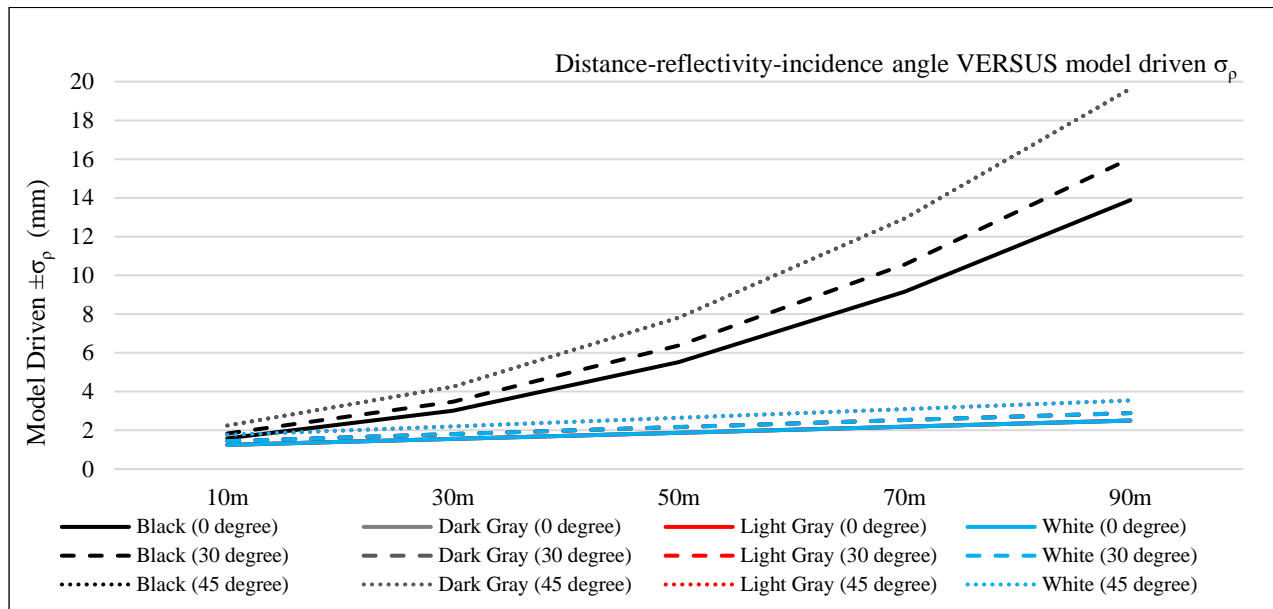


Figure 10. Model driven σ_p values for the Z+F 5010X scanner.

The model driven graphics of Figures 8-10 are the imitations of the data driven (empirical) graphics of Figures 4-6. They are practical and can be rendered with a less fieldwork. The formula of the range precision of the model driven approach fulfil the requirements mentioned above. The precision values σ_p of highly absorbent (black) objects are much higher when compared to dark gray, light gray and white objects. The precision values σ_p of non-black objects are almost linear and variations are very small. The precision values σ_p of non-black objects overlap expectedly, because the model driven approach treats the non-black objects as one class. In conclusion, the model driven σ_p values are compatible with the ones obtained by the data driven versions given in Figures 4-6.

4. VALIDATION OF THE PROPOSED POINT ERROR MODEL

In order to validate performance of the proposed error model, a test object was chosen and scanned with the aforementioned TLSs from the same stand point. This test object is a façade of a building (Figure 11) in the campus area of the Bulent Ecevit University (Zonguldak, Turkey).

The error ellipsoid parameters of each point for each scan were calculated by the described method. The validation of the proposed point error model was investigated using these ellipsoids. The error ellipsoids for Faro Focus 3D X330, Riegl VZ400 and Z+F 5010X derived point clouds are illuminated, respectively in the Figures 12, 13 and 14. The MATLAB programming environment was used for the computations. The VTK (Visualization Tool Kit) and C++ were used for the visualization purposes.

The test environment contains all the relevant parameters, varying scanner to object distances, incidence angles and surface reflectivity. The incidence angle is one of the majorly effecting parameters. As the incidence angle approaches to the extreme values, the corresponding error ellipsoids have elongated shapes. Oppositely, the ellipsoids resemble to spheres where the incidence angles approach to zero degree angles.

As shown in Figures 12, 13 and 14, our methodology successfully identifies the good quality laser points and the bad quality ones. This information is remarkably important when the millions of messy points are subject to object modeling, quality assessment, comparison and data fusion tasks.



Figure 11. The test object used for the validation.

5. CONCLUSIONS

A generic point error model was developed for the TLS derived point clouds. The complete workflow begins with estimation of angular a priori precision values, which are the scanner variant numbers. A static and repetitive measurement configuration is proposed. This step is followed by the determination of a priori range precision, in which an experimental set up is proposed. This set up is simple to implement in practice and can be applied for all TLS brands. Moreover, a model driven formula is developed for the range precision which is capable of parametrizing the distance from TLS to object, incidence angle, and surface reflectivity of the target object. The law of the error propagation was applied for the computation of the error ellipsoid parameters of the each point. Finally, an error ellipsoid can be attached to each point in the cloud. In the proposed model, the instrument-induced and the object space-induced random errors are factorized.

Performance of the presented model was validated in real world scenarios by using the point cloud data of three most recent TLS brands. The computed error ellipsoids indicate that the presented anisotropic error model works reasonable on the real data sets.

ACKNOWLEDGEMENTS

This research was funded by TUBITAK – The Scientific and Technological Research Council of Turkey (Project ID: 115Y239) and by the Scientific Research Projects of Bülent Ecevit University (Project ID: 2015-47912266-01).

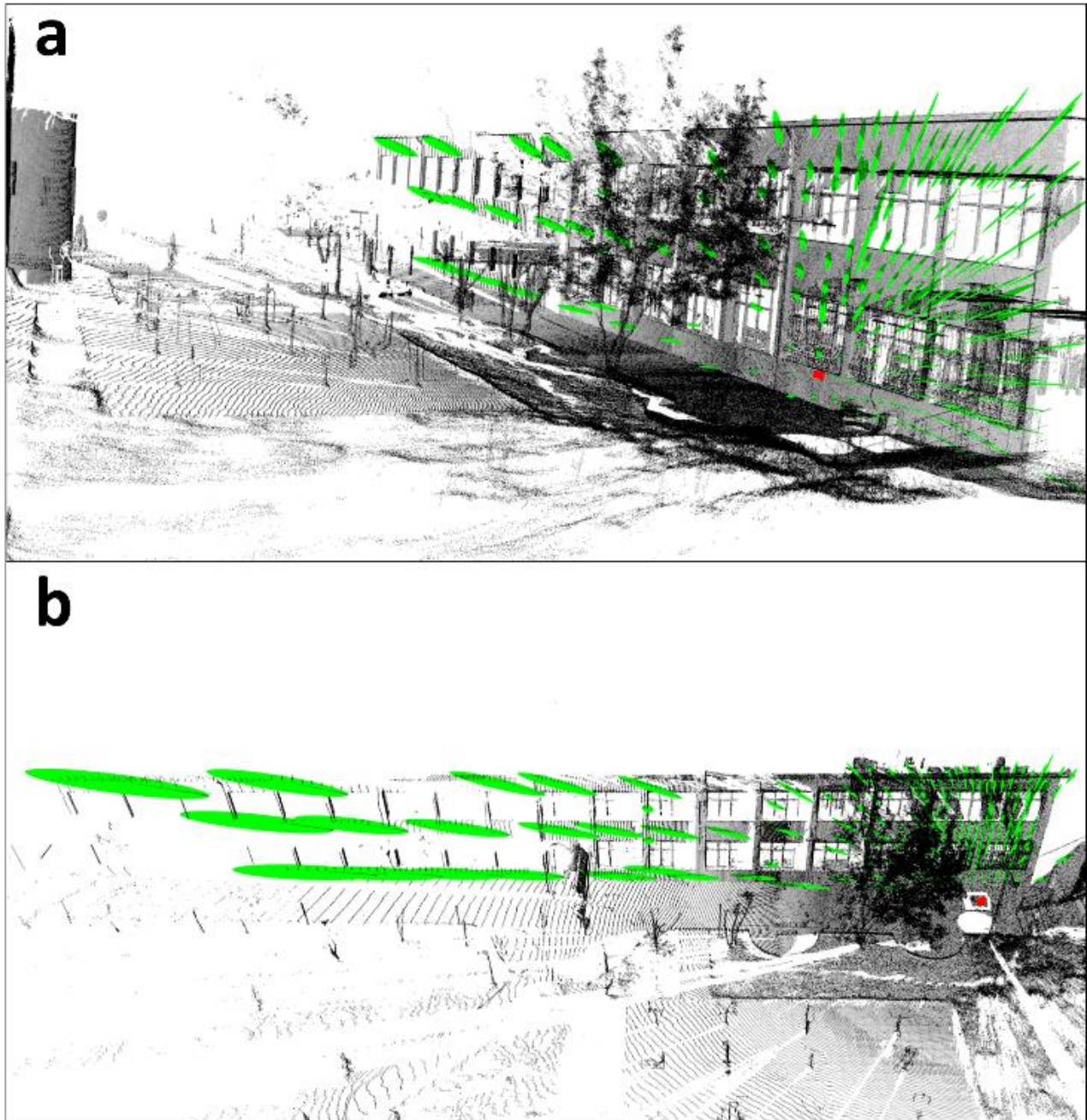


Figure 12. Two views (a) and (b) of a point cloud of the test object acquired by the Faro Focus 3D X330 scanner. The TLS station point is labelled by the red cube. The estimated error ellipsoids are represented in green color. The ellipsoids are plotted at every 200-th point and their sizes are exaggerated by factor 150 for a better visualization.

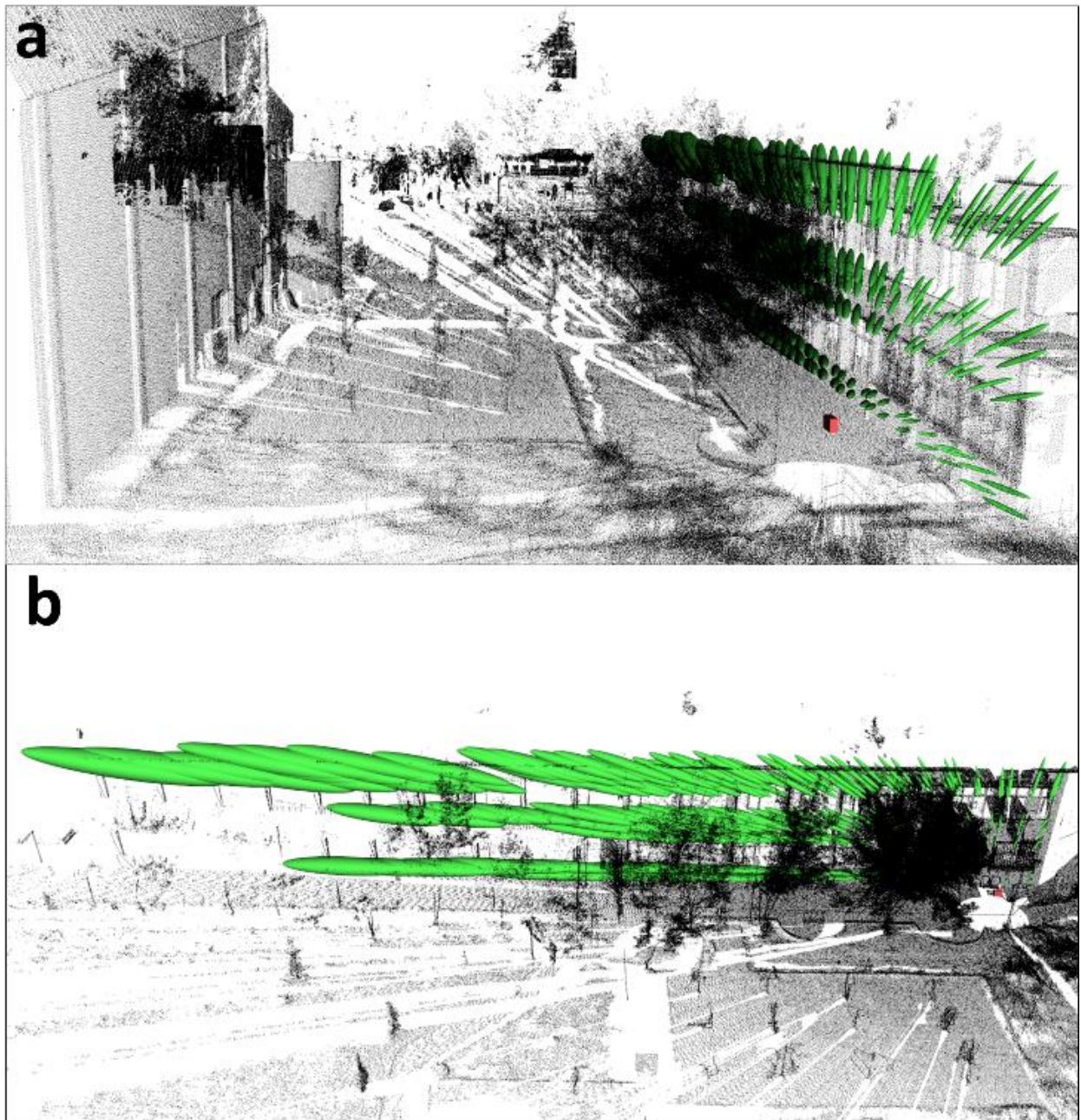


Figure 13. Two views (a) and (b) of a point cloud of the test object acquired by the Riegler VZ400 scanner. The TLS station point is labelled by the red cube. The estimated error ellipsoids are represented in green color. The ellipsoids are plotted at every 200-th point and their sizes are exaggerated by factor 100 for a better visualization.

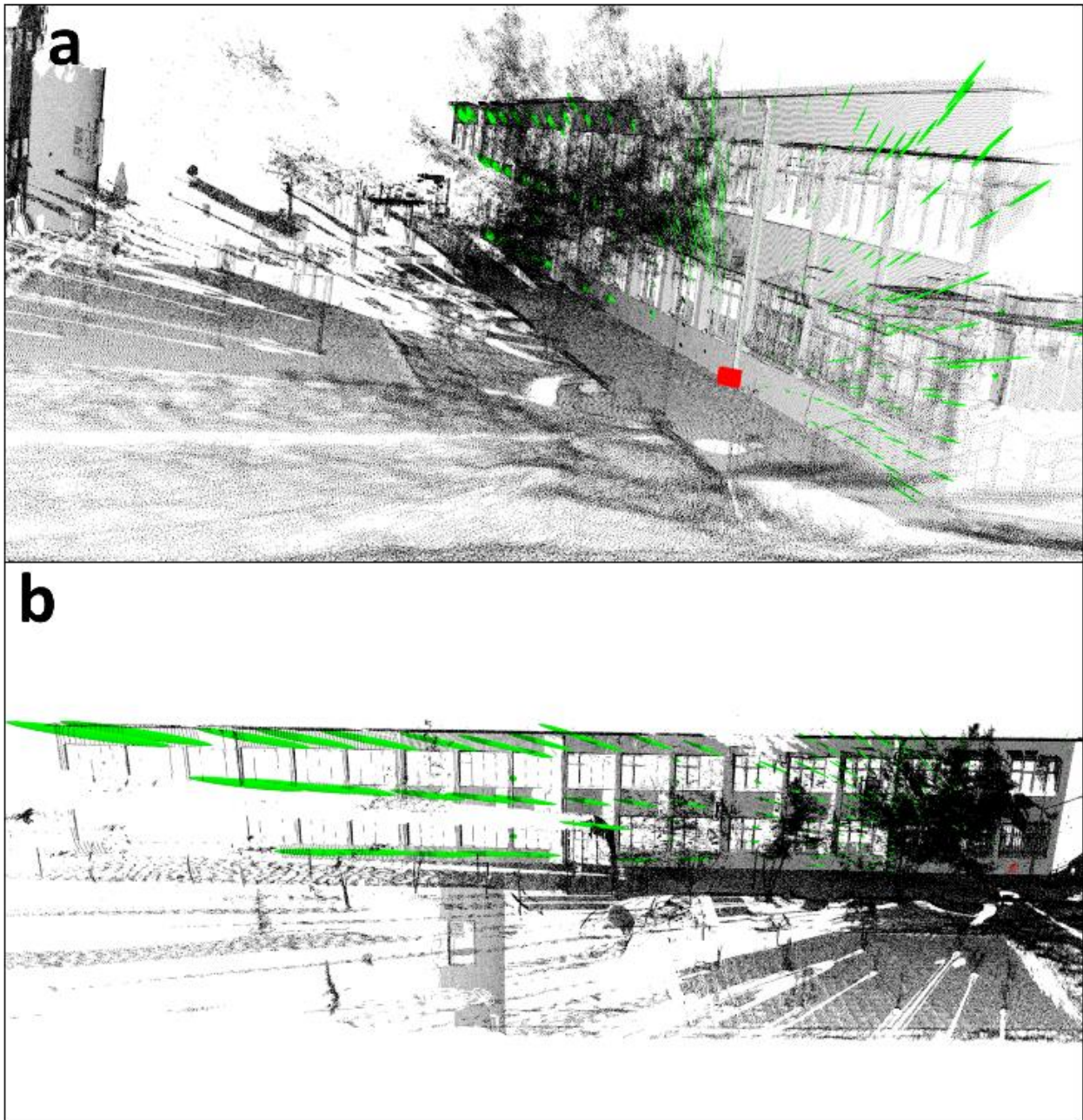


Figure 14. Two views (a) and (b) of a point cloud of the test object acquired by the Z+F 5010X scanner. The TLS station point is labelled by the red cube. The estimated error ellipsoids are represented in green color. The ellipsoids are plotted at every 200-th point and their sizes are exaggerated by factor 100 for a better visualization.

REFERENCES

- [1] Akca, D., Gruen, A., "Recent advances in least squares 3D surface matching," *Optical 3-D Measurement Techniques VII*, vol. II, 197-206 (2005).
- [2] Akca, D., Gruen, A., "Generalized Least Squares multiple 3D surface matching," *ISPRS Workshop on Laser Scanning 2007 and SilviLaser, International Archives of the Photogrammetry, Remote Sensing and Spatial Information Sciences*, vol. XXXVI, part 3 / W52, 1-7 (2007).
- [3] Akca, D., Remondino, F., Novák, D., Hanusch, T., Schrotter, G. and Gruen, A., "Recording and modeling of cultural heritage objects with coded structured light projection systems," *2nd International Conference on Remote Sensing in Archaeology*, 375-382 (2006).
- [4] Akca, D., Gruen, A., Alkis, Z., Demir, N., Breuckmann, B., Erduyan, I. and Nadir, E., "3D modeling of the Weary Herakles statue with a coded structured light system," *ISPRS Commission V Symposium, International Archives of the Photogrammetry, Remote Sensing and Spatial Information Sciences*, vol. XXXVI, part 5, 14-19 (2006).
- [5] Akca, D., Remondino, F., Novák, D., Hanusch, T., Schrotter, G. and Gruen, A., "Performance evaluation of a coded structured light system for cultural heritage applications," *Videometrics IX, Proc. of SPIE-IS&T Electronic Imaging, Proc SPIE 6491, 64910V-1-12* (2007).
- [6] Zhang, L., Kocaman, S., Akca, D., Kornus, W. and Baltsavias, E., "Test and performance evaluation of DMC images and new methods for their processing," *ISPRS Commission I Symposium, on CD-ROM* (2006).
- [7] Baltsavias E., Kocaman S., Akca D. and Wolff K., "Geometric and Radiometric Investigations of Cartosat-1 Data," *ISPRS Hannover Workshop on High Resolution Earth Imaging for Geospatial Information, on CD-ROM* (2007).
- [8] Matei, B., and Meer, P., "Optimal rigid motion estimation and performance evaluation with bootstrap," *IEEE Computer Society Conference on Computer Vision and Pattern Recognition 1*, 339-345 (1999).
- [9] Ohta, N., and Kanatani, K., "Optimal estimation of three-dimensional rotation and reliability evaluation," *ECCV'98: 5th European Conference on Computer Vision 1*, 175-187 (1998).
- [10] Williams, J. A., Bennamoun, M., and Latham, S., "Multiple view 3D registration: a review and a new technique," *IEEE SMC '99 Conference Proceedings*, 3, 497-502 (1999).
- [11] Hebert, M., and Krotkov, E., "3D Measurements From Imaging Laser Radars: How Good are They?," *Image and Vision Computing*, 10(3), 170-178 (1992).
- [12] Young Min, K., Chan, D., Theobalt, C., and Thrun, S., "Design and calibration of a multi-view TOF sensor fusion system," *IEEE Computer Society Conference on Computer Vision and Pattern Recognition Workshops*, 1-7 (2008).
- [13] Guehring, J., "Reliable 3D surface acquisition, registration and validation using statistical error models," *Proceedings Third International Conference on 3-D Digital Imaging and Modeling*, 224-231 (2001).
- [14] Okatani, I. S., and Deguchi, K., "A Method for Fine Registration of Multiple View Range Images Considering the Measurement Error Properties," *Computer Vision and Image Understanding*, 87(1-3), 66-77 (2002).
- [15] Sagawa, R., Oishi, T., Nakazawa, A., Kurazume, R. and Ikeuchi, K., "Iterative refinement of range images with anisotropic error distribution," *IEEE/RSJ International Conference on Intelligent Robots and Systems*, 1, 79-85 (2002).
- [16] Sagawa, R., Osawa, N., Echigo, T. and Yagi Y., "Real Time 3D Environment Modeling for a Mobile Robot by Aligning Range Image Sequences," *British Machine Vision Conference*, 330-339 (2005).
- [17] Sagawa, R., Osawa, N., and Yagi, Y., "A Probabilistic Method for Aligning and Merging Range Images with Anisotropic Error Distribution," *Third International Symposium on 3D Data Processing, Visualization, and Transmission*, 559-566 (2006).
- [18] Scaioni, M., "On the Estimation of Rigid-Body Transformation for TLS Registration," *Int. Arch. Photogramm. Remote Sens. Spatial Inf. Sci.*, XXXIX-B5, 601-606 (2012).
- [19] Bae, K.-H., Belton, D., and Lichti, D. D., "A Closed-Form Expression of the Positional Uncertainty for 3D Point Clouds," *IEEE Trans. Pattern Anal. Mach. Intell.*, 31(4), 577-590 (2009).
- [20] Soudarissanane, S., Lindenbergh, R., Menenti, M. and Teunissen, P., "Scanning geometry: Influencing factor on the quality of terrestrial laser scanning points," *ISPRS Journal of Photogrammetry and Remote Sensing*, 66(4), 389-399 (2011).

- [21] Grant, D., Bethel, J., and Crawford, M., "Point-to-plane registration of terrestrial laser scans," *ISPRS Journal of Photogrammetry and Remote Sensing*, 72, 16-26 (2012).
- [22] Baselgia, C., Bosse, M., Zlot, R. and Holenstein, C., "Solid model reconstruction of large-scale outdoor scenes from 3D LiDAR data," *Field and Service Robotics: Results of the 8th International Conference*, 541-554 (2014).
- [23] Chen, X., Hua, X., Zhang, G., Wu, H., Xuan, W. and Li, M., "Evaluating point cloud accuracy of static three-dimensional laser scanning based on point cloud error ellipsoid model," *Journal of Applied Remote Sensing*, 9(1), 095991 (2015).
- [24] Chen, X., Zhang, G., Hua, X. and Xuan, W., "An average error-ellipsoid model for evaluating TLS point-cloud accuracy," *The Photogrammetric Record*, 31(153), 71-87 (2016).
- [25] Schaer, P., Skaloud, J., Landtwing, S. and Legat, K., "Accuracy Estimation for Laser Point Cloud Including Scanning Geometry," *5th International Symposium on Mobile Mapping Technology*, (2007).
- [26] Mezian, C., Vallet, B., Soheilian, B. and Paparoditis, N., "Uncertainty Propagation for Terrestrial Mobile Laser Scanner," *Int. Arch. Photogramm. Remote Sens. Spatial Inf. Sci.*, XLI-B3, 331-335 (2016).
- [27] Wujanz, D., Burger, M., Mettenleiter, M. and Neitzel, F., "An intensity-based stochastic model for terrestrial laser scanners," *ISPRS Journal of Photogrammetry and Remote Sensing*, 125, 146-155 (2017).
- [28] Ingensand, H., "Metrological aspects in terrestrial laser-scanning technology," *Proceedings of the 3rd IAG/12th FIG symposium*, (2006).
- [29] Schulz, T., [Calibration of a Terrestrial Laser Scanner for Engineering Geodesy], *Institute of Geodesy and Photogrammetry of the ETH Zurich* (2008).
- [30] Parian, J. A., and Gruen, A., "Integrated laser scanner and intensity image calibration and accuracy assessment," *Proceedings of the ISPRS Workshop Laser scanning 2005*, XXXVI, 18-23 (2005).
- [31] Chow, J. C., Lichti, D. D., and Teskey, W. F., "Self-calibration of the Trimble (Mensi) GS 200 terrestrial laser scanner," *Proceedings of the International Archives of Photogrammetry, Remote Sensing and Spatial Information Sciences*, 38, 161-166 (2010).